JOC The Journal of Organic Chemistry
Cite This: J. Org. Chem. 2020, 85, 118−128
Article
pubs.acs.org/joc

Mechanical Fixation by Porphyrin Connection: Synthesis and Transport Studies of a Bicyclic Dimer

Patrick Zwick,[†] Kevin J. Weiland,[†] Juraj Malinčík,[†] Davide Stefani,[‡] Daniel Häussinger,[†] Herre S. J. van der Zant,[‡] Diana Dulić,[§] and Marcel Mayor*[,†,∥,⊥]

[†]Department of Chemistry, University of Basel, St. Johanns-Ring 19, 4056 Basel, Switzerland
[‡]Kavli Institute of Nanoscience, Delft University of Technology, Lorentzweg 1, 2628 CJ Delft, The Netherlands
[§]Department of Physics and Department of Electrical Engineering, Faculty of Physicaland Mathematical Sciences, University of Chile, Avenida Blanco Encalada 2008, Santiago 8330015, Chile
[∥]Institute for Nanotechnology (INT), Karlsruhe Institute of Technology (KIT), P.O. Box 3640, 76021 Karlsruhe, Germany
[⊥]Lehn Institute of Functional Materials (LIFM), School of Chemistry, Sun Yat-Sen University (SYSU), 510275 Guangzhou, China

Supporting Information

ABSTRACT: The bowl-shaped, 3-fold interlinked porphyrin dimer **2** was obtained in respectable yields during macrocyclization attempts. Its bicyclic structure, consisting of a macrocycle made of a pair of acetylene interlinked tetraphenylporphyrins which are additionally linked by a C−C bond interlinking two pyrrole subunits, has been confirmed spectroscopically (2D-NMR, UV/vis, HR-MALDI-ToF MS). Late-stage functionalization provided the structural analogue **1** with acetyl-protected terminal thiol anchor groups enabling single molecule transport investigations in a mechanically controlled break junction experiment. The formation of single-molecule junctions was observed, displaying large variations in the observed conductance values pointing at a rich diversity in the molecular junctions.

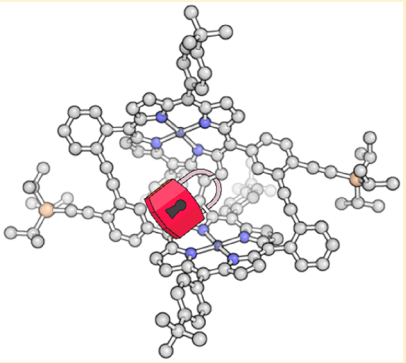

INTRODUCTION

Molecules are the smallest building blocks still providing the structural diversity and integrity required to integrate a particular function by the spatial arrangement of their atoms. In combination with the skills of chemistry in molecular design and synthesis making the targeted structures available in enormous numbers of identical copies, they became the object of interest as potential functional subunit in electronics. While the visionary concept was suggested almost 5 decades ago by the pioneering paper of Aviram and Ratner, hypothesizing the rectifying behavior of a virtual single molecule junction,[1] mainly the developments in experimental physics enabled the realization of single molecule junctions.[2] The increasing experimental skills moved the focus of interest from theoretical hypotheses to electric circuits comprising single molecules. The parallel blossom of the three required scientific disciplines (synthetic chemistry,[3] experimental physics,[4] and theoretical simulation[5]) enables the structure−property relationships required to evaluate both the potential and the limitation of molecular electronics.[6]

While fundamental transport−property correlations corroborated the single-molecule nature of the junction[7] and first electronic functions like rectifying[8] or switching[9] were successfully implemented, we became recently interested in mechanosensitive molecular junctions. First, single-molecule junctions with mechanosensitive transport features[10−12] or redox properties[13] were reported. The variation of the single-molecule transport features was either due to a mechanically triggered alteration of the spin state[14] or the manipulation of the spatial conformation of two neighboring π-systems in close proximity. The latter has been rationalized by quantum interference phenomena and was observed in bimolecular junctions due to π-stacking[15] as well as in covalently interlinked π-systems like [2.2]paracyclophanes.[16]

Porphyrins play a key role in nature's machinery converting sun light into chemical energy,[17] and their adjustable electronic and optical properties[18−20] make particularly appealing building blocks in molecular electronics and molecular devices. Consequently, electronic transport studies of model compounds based on porphyrin subunits have been reported; e.g., molecular wires,[21,22] tapes,[23] and even the anchoring groups for gold electrodes have been altered.[24] Recently, the variations of transport paths in single porphyrin junctions recorded in a mechanically controlled break junction (MCBJ) device were systematically analyzed by an unsupervised clustering algorithm,[25] and the study revealed the potential of porphyrin

Special Issue: Functional Organic Materials
Received: August 27, 2019
Published: November 5, 2019

DOI: 10.1021/acs.joc.9b02327
J. Org. Chem. 2020, 85, 118−128

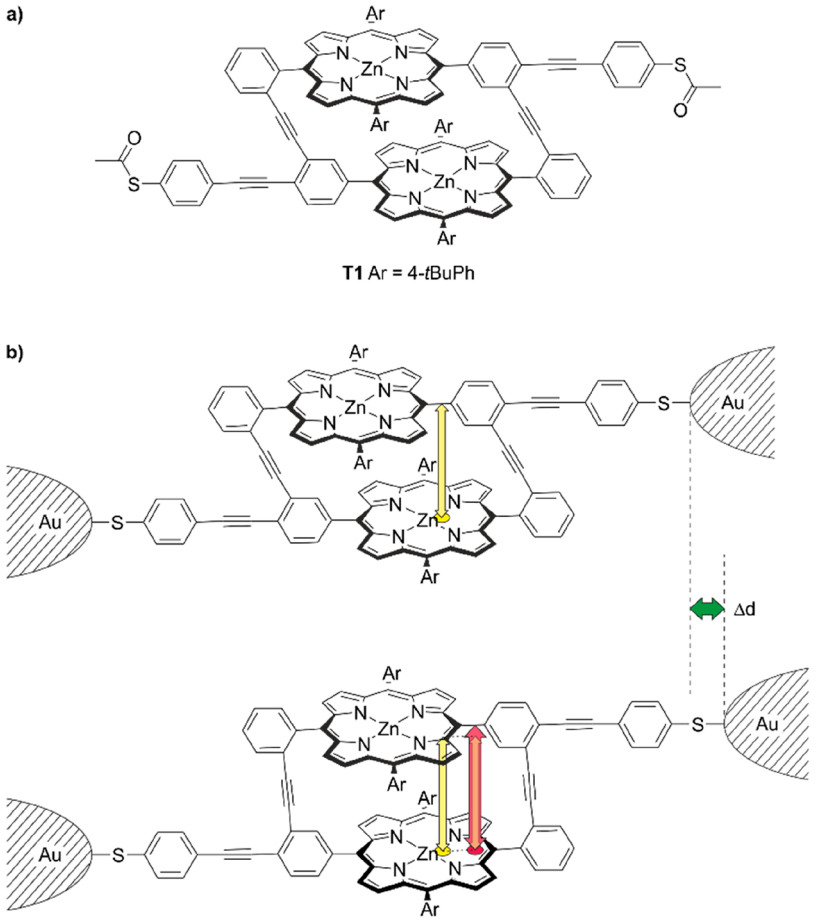

Figure 1. (a) Porphyrin cyclophane **T1** as initial target structure. (b) Hypothesized variation of the spatial arrangement of both porphyrins triggered by the electrode displacement. In the oligophenylenethinylen macrocycle resembling a parallelogram, the increase in the distance of both anchor groups translates in an increased distance of both porphyrin planes together with their lateral shift. As guide for the eye, the initial yellow arrow and the touching points of the distance arrows are displayed in the bottom sketch of Figure 1b).

derivatives as well behaved and reproducible model compounds for single molecule junctions.

Motivated by these promising results, our interest moved toward macrocyclic architectures comprising porphyrins, with the intention to manipulate the interaction between the porphyrins in a junction mechanically. The first target structure along these lines was the porphyrin cyclophane **T1** displayed in Figure 1a. The macrocyclic phenyl ethynylene framework resembles a parallelogram with two zinc(II)porphyrins facing each other in an offset cofacial orientation. Both porphyrin levels of the macrocycle are decorated with an acetyl masked thiol anchor group, with the intention to immobilize the macrocycle in a MCBJ experiment with covalent S−Au bonds. The chemically stable fixation of the structure inside the electrodes' gap is crucial to enable the mechanical manipulation of the molecular junction. Upon immobilization, the spatial arrangement of both cofacially arranged porphyrin subunits, and thus also the fraction of the transport current arising from the spatial proximity of both porphyrin systems, are expected to depend on the electrode spacing. As sketched in Figure 1b, an increase of the electrode spacing by Δd (green arrow) should not only result in an increased spacing between both porphyrin levels (difference between red and yellow arrow) but also in the relative displacement of both porphyrin subunits with respect to each other (as a guide for the eye the touching points of the distance arrows are displayed in the lower porphyrin plane).

In this work, we report our synthetic efforts toward the macrocyclic porphyrin cyclophane **T1**, which we were not able to isolate so far. However, in our attempts to form the macrocycle of **T1**, we observed the formation of an unexpected additional carbon−carbon bond between both porphyrin planes, resulting in the 3-fold interbridged porphyrin architecture **2**, as a precursor of the anchor group decorated bowl-shaped porphyrin dimer **1** (see Figure 2). The interesting bicyclic porphyrin architecture **2** was isolated, and its structural identity was corroborated by means of 2-dimensional nuclear magnetic resonance spectroscopy (2D-NMR), high-resolution mass spectrometry (HR-MS), and UV−vis spectroscopy. Additionally, **2** was investigated with computational methods at the B3LYP/LanL2DZ level of theory (for details regarding the calculations, see the Supporting Information). The calculation supports the bowl shape of the molecule. The strain introduced by additional $\beta-\beta$ linkage is accommodated by bending of the porphyrins from their usual planar conformation (additional information, e.g., calculated distances and angles can be found in Figure S36).

The fixation by an additional C−C bond between both porphyrin subunits in **1** was expected to handicap its mechanosensitivity. It remained, however, an interesting model compound to investigate the transport features and,

DOI: 10.1021/acs.joc.9b02327
J. Org. Chem. 2020, 85, 118−128

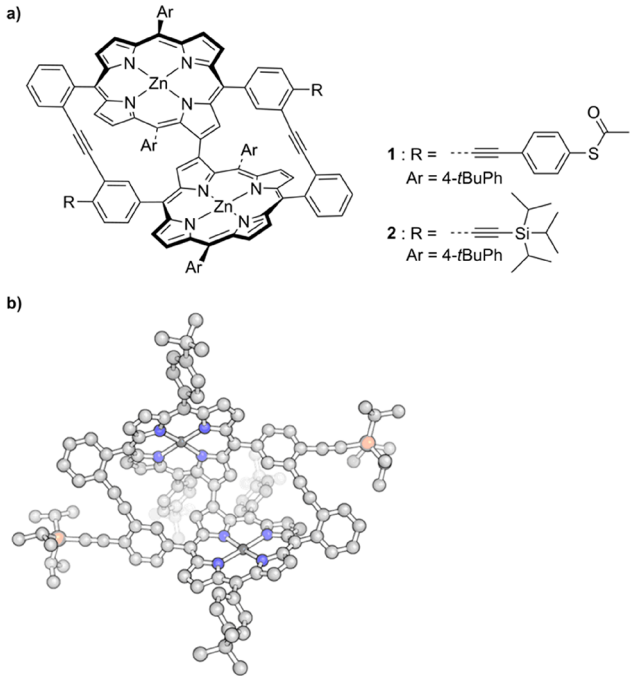

Figure 2. (a) Structures of the 3-fold interlinked polycyclic porphyrin architectures **1** and **2**. (b) Calculated (geometry optimized by B3LYP/LanL2DZ)[26] ball-and-stick model of the porphyrin bicyclic dimer **2** displaying the bowl-shaped arrangement of the porphyrin architecture.

thus, also the suitability of complex multilevel porphyrin architectures for MCBJ experiments. Hence, the transport properties of the bowl-shaped porphyrin bicycle **1** were analyzed by immobilization in MCBJ experiments, applying both fast- and self-breaking techniques.

RESULTS AND DISCUSSION

Retrosynthesis. The synthetic plan toward **T1** is displayed in Scheme 1, with the macrocyclization of two molecules of **3** in a 2-fold Sonogashira–Hagihara reaction as key step. The macrocyclization was expected to be particularly challenging. The search for suitable (pseudo) high dilution conditions favoring macrocyclization over oligo- and polymerization became challenging with palladium and copper catalysts required to activate both functional groups engaged in the coupling reaction. After successful cyclization, late-stage liberation of the peripheral acetylenes and subsequent decoration with subunits exposing the required anchor groups was expected to provide the target porphyrin cyclophane **T1**.

The highly functionalized porphyrin monomer **3**, exposing with acetylene and bromine both functional groups for the macrocyclization, was divided into literature known 2,2′-((4-(*tert*-butyl)phenyl)methylene)bis(1*H*-pyrrole),[27] commercially available 2-bromobenzaldehyde and **4**, which itself should be available by a sequence of Sonogashira–Hagihara cross-coupling reactions profiting from the variation in reactivity of halide substituents from commercially available 4-bromo-3-iodobenzaldehyde.

Synthesis. The diacetylene benzaldehyde **4** was found to be easily accessible over two subsequent Sonogashira–Hagihara cross-coupling reactions from 4-bromo-3-iodobenzaldehyde. First, the more reactive iodine was substituted by trimethylsilyl (TMS) acetylene at room temperature, providing **5** in 85%. At an elevated temperature of 80 °C, the bromine was substituted by triisopropylsilyl (TIPS) acetylene, providing the benzaldehyde building block **4** with an overall yield of 69% over both coupling steps on a 20 g scale.

The porphyrin **6** was condensed from 2,2′-((4-(*tert*-butyl)phenyl)methylene)bis(1*H*-pyrrole),[28] 2-bromobenzaldehyde, and **4** (see Scheme 2). Trifluoroborane diethyl etherate was used as a Lewis acid in a 10 mM solution of the starting

Scheme 1. Retrosynthetic Strategy to the Porphyrin Cyclophane T1 over Key Intermediates T2, 3, and 4

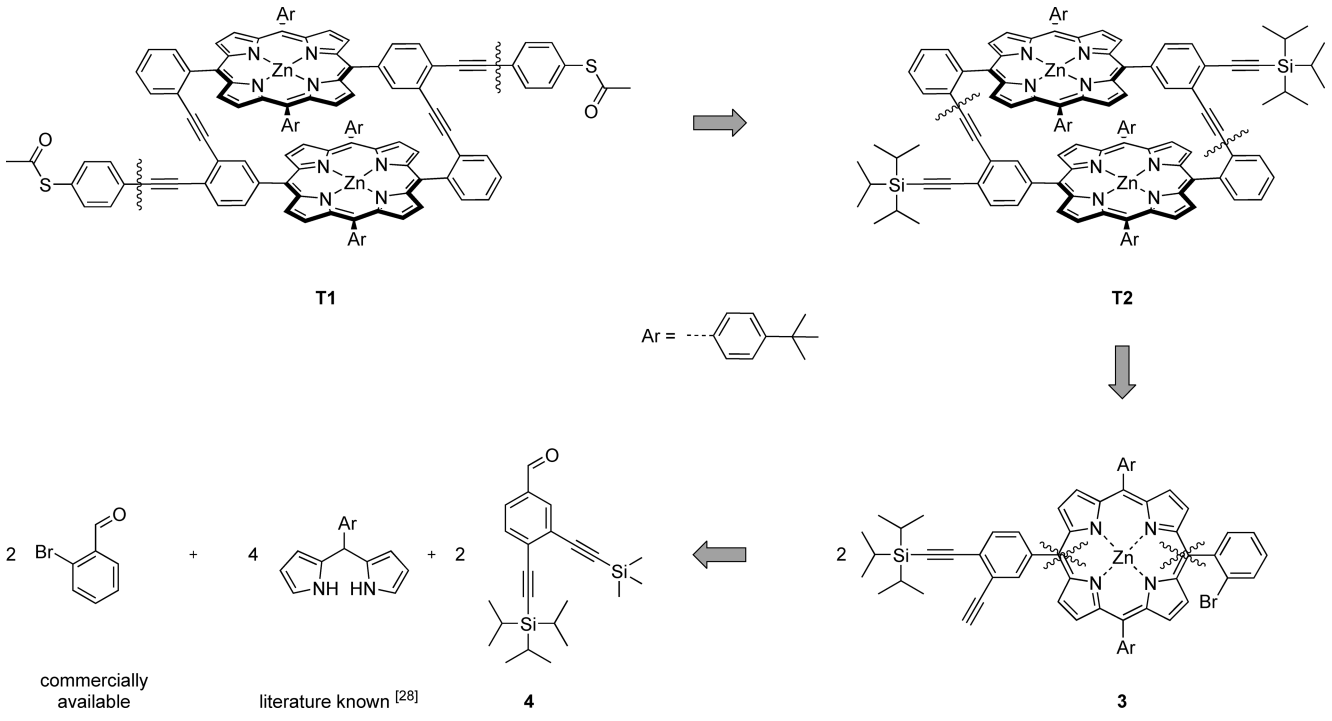

DOI: 10.1021/acs.joc.9b02327
J. Org. Chem. 2020, 85, 118–128

Scheme 2[a]

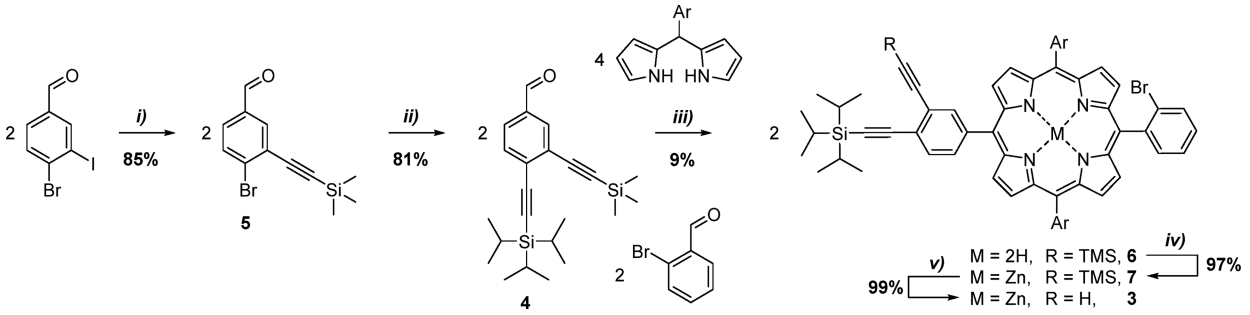

[a]Key: (i) TMS-CCH, $Pd(PPh_3)_2Cl_2$, CuI, piperidine/THF (1:3), rt, 3 h; (ii) TIPS-CCH, $Pd(PPh_3)_2Cl_2$, CuI, piperidine/$C_6H_5CH_3$ (1:3), 80 °C, 2 h; (iii) (1) $BF_3{\cdot}OEt_2$, CH_2Cl_2, −10 °C, 15 min, (2) DDQ, CH_2Cl_2, rt, 30 min; (iv) $Zn(OAc)_2$, CH_2Cl_2/CH_3OH (1:1), rt, 1 h; (v) K_2CO_3, CH_2Cl_2/CH_3OH (1:1), rt, 2 h.

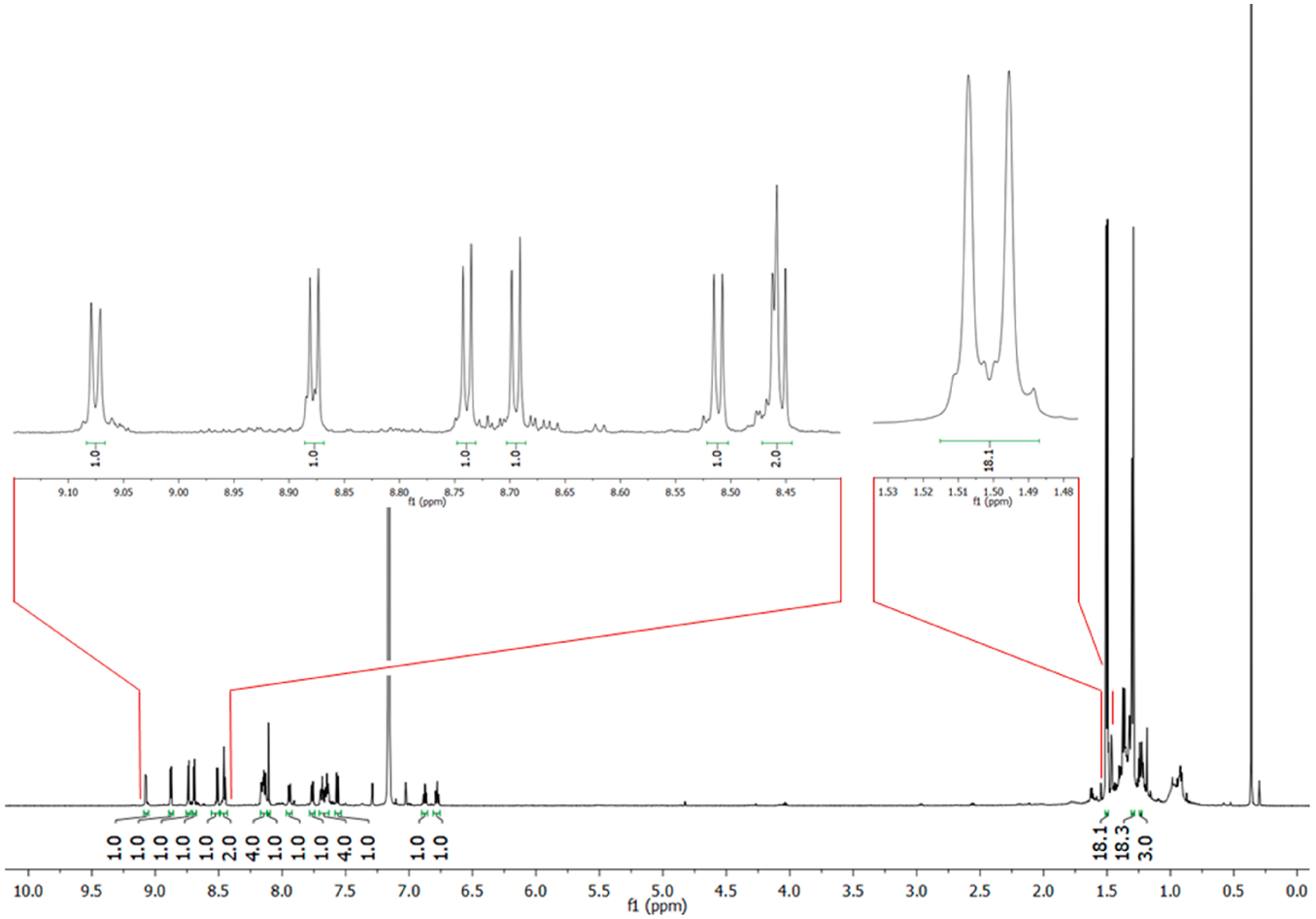

Figure 3. ^1H NMR spectrum of **2** recorded in C_6D_6 at room temperature with a 600 MHz proton frequency.

materials in CH_2Cl_2 at −10 °C (20 mM for 2,2′-((4-(*tert*-butyl)phenyl)methylene)bis(1*H*-pyrrole)). The reaction mixture was oxidized by 2,3-dichloro-5,6-dicyano-1,4-benzoquinone (DDQ) after 15 min. It is noteworthy that the yields dropped significantly for longer reaction times and higher temperatures (e.g., 2% for 1 h at rt), where increased scrambling of the condensed intermediates prior to aromatization was observed. The porphyrin **6** was isolated in 9% yield on a 500 mg scale in a multistep protocol. The crude reaction mixture was first filtered through a silica plug using CH_2Cl_2 as eluent. The crude was further purified by a size exclusion column (Bio Beads SX-3 in toluene) where the fractions comprising the target structure were identified by thin layer chromatography (TLC; R_f(**6**) = 0.55 for SiO_2, ethyl acetate/toluene/cyclohexane: 1/1/25) and collected. The analytically pure **6** was finally obtained by precipitation from a concentrated CH_2Cl_2 solution by the addition of CH_3OH.

The free-base porphyrin **6** was metalated to make it suitable for standard Sonogashira−Hagihara cross-coupling reactions toward **T2**. Treatment of a solution of **6** in CH_2Cl_2/CH_3OH (1:1) with an excess of $Zn(OAc)_2$ (5 equiv) afforded **7** in **97%** yield. Subsequent deprotection of the TMS acetylene with K_2CO_3 in CH_2Cl_2/CH_3OH (1:1) gave **3** in **99%** yield. All three porphyrin monomers **6**, **7**, and **3** were characterized by

DOI: 10.1021/acs.joc.9b02327
J. Org. Chem. 2020, 85, 118−128

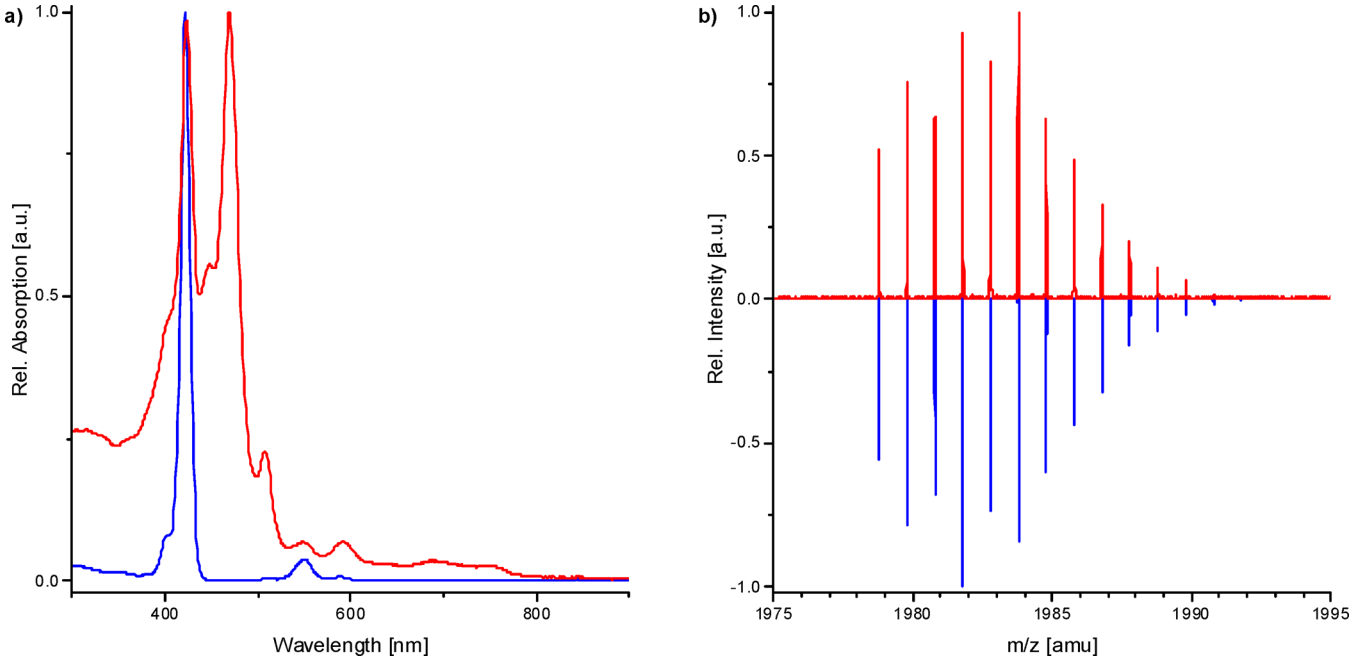

Figure 4. (a) normalized UV−vis spectra of **3** (blue) and **2** (red) in CH_2Cl_2, displaying the substantial Soret-band splitting observed with **2**. (b) High-resolution MALDI mass spectrum of **2** (red, normalized to 1) and simulation of the expected isotopic distribution (blue, normalized to −1).

Scheme 3. Dimerization of the Precursor 3 to the Bowl-Shaped Porphyrin Dimer 2[a]

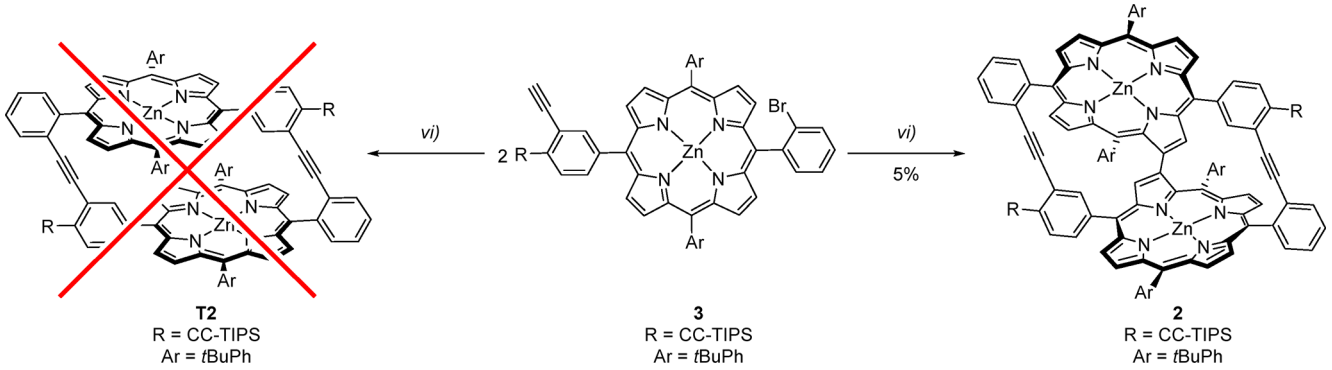

[a]Key: (vi) $Pd(PPh_3)_4$, dppf, CuI, $NEt_3/C_6H_5CH_3$ (1:3), 110°C, 2 d.

thin-layer chromatography (TLC), melting point, ^{1}H NMR and UV−vis spectroscopy, MALDI-ToF mass spectrometry, as well as elemental analysis. However, due to the low solubility of **3**, $^{13}C\{^1H\}$-NMR spectroscopy was only performed for **6** and **7**.

The precursor **3** was exposed to a large variety of Sonogashira−Hagihara conditions. Based on our experience, we started with slightly elevated temperatures between 60 and 90 °C and with catalytic amounts (5 to 10 mol %) of Pd(0) and Cu(I) salts with a variety of ligands. Neither variation of the reaction solvents and bases nor the rigorous exclusion of oxygen yielded promising results. In all attempts, exclusively larger oligomers and/or debrominated precursors were detected by matrix-assisted laser desorption time-of-flight mass spectrometry (MALDI-ToF-MS) together with unidentified degradation products. Driven by the hope for finding of suitable macrocyclization conditions, the harshness of the reaction conditions was increased steadily. Indeed, when **3** was dissolved as 500 μM solution in a mixture of toluene and triethylamine (NEt_3), equimolar amounts of $Pd(PPh_3)_4$ and 1,1′-bis(diphenylphosphino)ferrocene (dppf) were added together with 1.1 equiv of CuI and the reaction mixture was stirred at 110 °C for 2 d in a closed Schlenk flask, reaction products in a promising mass range were detected. However, the parallel formation of oligomers and small amounts of homocoupled side products rendered the isolation of the compound comprising the interesting mass challenging. The reaction mixture was filtered on a silica short plug using toluene as eluent. Higher oligomers and monomeric porphyrin species were removed by two subsequent size exclusion columns (SX-1 and SX-3 Bio Beads in toluene). The remaining mixture was subjected to automated GPC, and the separated fractions were analyzed by MALDI-ToF-MS. The crude product was subjected to column chromatography with freshly distilled solvent, and the compound of interest was isolated in 5% yield.

Surprisingly, the ^{1}H NMR spectrum (Figure 3) of the isolated compound disqualified the targeted cyclophane **T2** as its structure. Immediately apparent was the splitting of the *tert*-butyl signals into two equally weighted singlets, instead of the

DOI: 10.1021/acs.joc.9b02327
J. Org. Chem. 2020, 85, 118−128

Scheme 4[a]

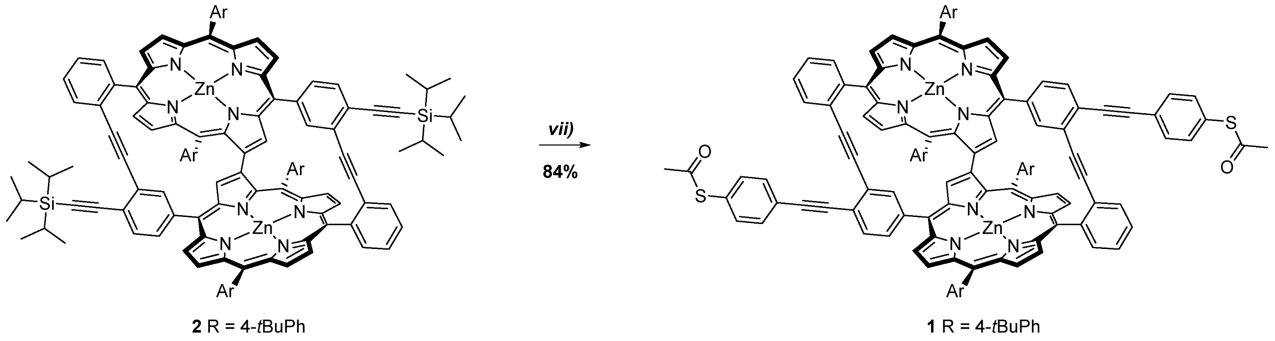

[a]Key: (vii) (1) TBAF, THF, rt, 1 h, (2) *S*-(4-iodophenyl) ethanethioate, $Pd(PPh_3)_4$, CuI, NEt_3/THF (1:3), rt, 2 h.

single peak expected for the symmetry of **T2**. In the aromatic region, an odd number of downfield shifted signals of the β-protons of the porphyrins' pyrrole subunits were found. While six signals displayed the doublet expected for the coupling with their neighbors, the seventh signal was a singlet indicating the absence of a proton-bearing next neighbor. The absence of a coupling partner was further corroborated by $^1H-^1H$ COSY-NMR spectroscopy (see Figure S25). The molecular signal of the isolated compound recorded by high-resolution mass spectrometry was with m/z = 1978.7912 (Figure 4b), two mass units shorter than the value expected for **T2** (m/z = 1980.8065), suggesting that the two missing β-protons were not substituted by any NMR inactive nuclei, but pointing at a newly formed intramolecular C−C bond interlinking the pyrrole subunits of both porphyrins. In the UV/vis spectrum of the isolated compound (Figure 4a), a Soret-band splitting of 50 nm (global maxima at 422 and 472 nm) was observed, pointing at exciton coupling of a spatially fixed porphyrin pair.[29,30]

The structure supported by the analytical data is the 3-fold interlinked porphyrin dimer **2** (Scheme 3), in which an additional C−C bond is formed between the β-positions of a pyrrole subunit from each porphyrin. Such formations of $\beta-\beta$ linkages are known to form under strong Lewis acidic conditions or, in rare cases, promoted by transition metals, including palladium.[31] They typically require high structural preorganization as exemplified for porphyrin tapes and sheets.[32−35] We surmise that this additional linking occurs immediately after closing of the cyclophane **T2**, promoted by the proximity of the porphyrins. This might explain why we did not find experimental evidence for **T2**. The additional C−C bond breaks the symmetry of the compound and forces the porphyrins to adapt to a bowl-shaped structure.

The topology of **2** was unambiguously determined by means of 2D-NMR experiments. The full characterization with the assignment of each proton and carbon signal can be found in the Supporting Information (see Figure S30). A slight concentration dependence of the proton chemical shifts pointed at stacking behavior even in aromatic solvents like deuterobenzene. To unambiguously prove the dimeric nature of **2**, its diffusion coefficient was determined ($3.64(4) \times 10^{-10}$ m^2/s) by pulsed field gradient spin echo (PFGSE) experiment and calibrated with the diffusion coefficient of compound **3** recorded under identical conditions ($4.93(2) \times 10^{-10}$ m^2/s) (see Figure S29 and Table S1). From the ratio of the two diffusion coefficients the hydrodynamic radius r_H of **2** was calculated using the Stokes−Einstein equation to be 1.35 times larger than the r_H of **3**, resulting in a 2.48 times larger molecular weight including the first solvation sphere which is in reasonable agreement with the proposed dimeric structure.

By late-stage peripheral functionalization, a small sample of the 3-fold interlinked porphyrin bicycle was optimized for single-molecule junction experiments. The terminal acetylenes of **2** were liberated by treatment with an excess of tetra-*n*-butylammonium fluoride (TBAF) in wet THF. After 1 h, the mixture was filtered over silica, and the solvent was evaporated under reduced pressure. The remaining crude reaction product was dried at high vacuum and redissolved in dry THF. The degassed solution was transferred into a flask containing NEt_3, 3 equiv of *S*-(4-iodophenyl)ethanethioate, 5 mol % $Pd(PPh_3)_4$, and 6 mol % CuI. After the solution was stirred for 2 h at room temperature, monitoring by TLC indicated spot to spot conversion. The reaction mixture was filtered through a silica short plug with CH_2Cl_2 as eluent. Size-exclusion chromatography (Bio Beads SX-3 in toluene) provided the desired porphyrin bicycle **1** in 84% yield over both steps (see Scheme 4). Due to both the minute dimension of the sample and the limitations in solubility, only TLC, high-resolution MALDI-ToF-MS, and UV/vis are available as data characterizing the 3-fold interlinked bicycle **1** exposing acetyl-protected thiol anchor groups.

Current Transport Investigation. The suitability of the bicyclic porphyrin dimer **1** for transport measurement in a single-molecule junction was investigated in a MCBJ experiment (Figure 5). Details of this technique have been published previously,[36−38] and the method is only presented briefly. A lithographically fabricated thin gold wire was deposited on a

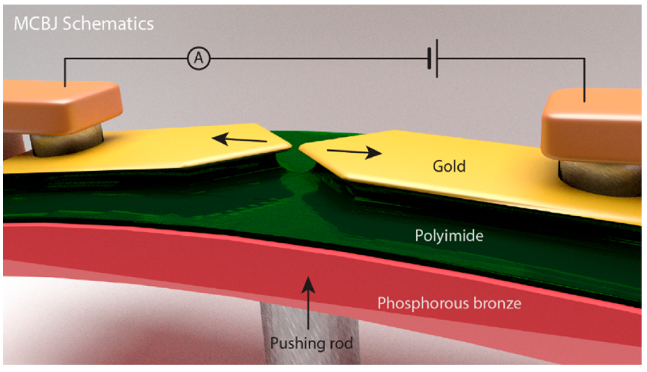

Figure 5. Sketch of a mechanically controlled break junction (MCBJ) experiment displaying the multilayer architecture and the basic components.

DOI: 10.1021/acs.joc.9b02327
J. Org. Chem. 2020, 85, 118−128

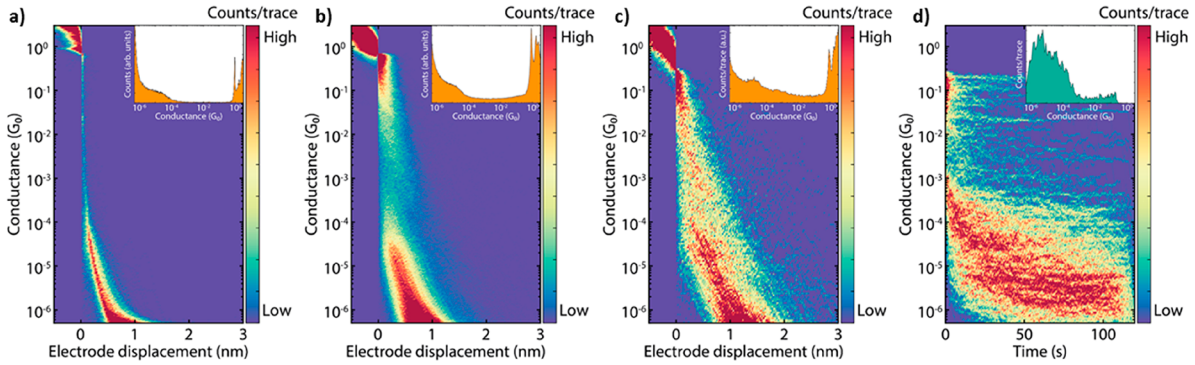

Figure 6. Two-dimensional histograms built before (a) and after (b and c) drop-casting a CH_2Cl_2 solution containing **1**. The insets show the one-dimensional conductance histogram. The histogram in panel a was built from 2000 consecutive CDTs, while the one in panel b was built from the 10000 CDTs collected after the deposition of **1**. The histogram in panel c was built from the 890 CDTs selected by the clustering algorithm. (d) Two-dimensional histogram built from 704 consecutive conductance-time traces collected with the self-breaking method. Insets: one-dimensional conductance histograms belonging to the panels.

flexible substrate. The center of the wire consisted of a 100 nm wide constriction that was suspended after etching the supporting polyimide, with an O_2 plasma. The flexible substrate was clamped between two lateral supports in a three-point bending mechanism and deformed by driving a pushing rod connected to a cantilever into it. Upon bending of the substrate, the gold wire was stretched until the breaking of the wire results in two sharp electrodes. The flexibility of the substrate allowed the adjustment of the electrode separation by the mechanical positioning of the pushing rod. The geometrical design of the samples was such that the vertical displacement of the cantilever was converted into a horizontal electrode displacement, which resulted in a subnanometer control over the electrodes separation. By relaxation of the bending the two broken extremities could be fused again reforming the gold wire. This process could be repeated several thousand times without a noticeable aging of the wire, providing the vast amount of data required for meaningful statistical analyses. In this study, a 5 mM solution of **1** in CH_2Cl_2 was drop casted on the junction after the characterization of the bare device. Once the solvent was evaporated, the above-described breaking and making process was repeated 10000 consecutive times, and the breaking traces were collected without any data selection giving a two-dimensional conductance versus electrode displacement histogram. The molecular junction formation has been operated in two different modes. The fast-breaking mode[39] forming quickly one electrode pair after the other and the self-breaking mode,[40] allowing the electrodes to relax screening for particular stable configurations in the molecular junction.

In the fast-breaking mode, the conductance was measured as the distance between the electrodes was progressively increased until the conductance dropped below the detection level. The electrode displacement speed was typically 3−9 nm/s. In 9% of the 10000 recorded consecutive conductance-displacement traces (CDTs), a plateau-like feature was observed (Figure 6c). It is noteworthy that these 890 CDTs reflecting a molecular feature have been selected by an automated clustering algorithm[40] which was dividing the 10000 CDTs (Figure 6b) into five classes. The plateaus observed in the 9% of the CDTs were at various conductance levels and occasionally longer than 2 nm, excluding through space tunneling as potential origin of the CDTs. To demonstrate the difference between these molecular junctions (Figure 6c) and empty junctions in the histograms, the CDTs of the same device before deposition of **1** are displayed in Figure 6a). The remaining four classes displayed CDTs without significant features and were attributed to empty junctions. The one-dimensional conductance histogram (inset of Figure 6c) displayed rather a continuous increase than a well-defined peak representing the conductance of the molecule in the junction. The absence of such a preferred conductance value points at a large variety of molecular configurations inside the junction with different conductance characteristics.

In order to assess the most stable configurations in the junction, self-breaking measurements were performed on the same sample. In this method, the MCBJ junction was initially stretched to a few-atom width and allowed to self-break by its surface tension to form atomically sharp electrodes. The electrodes were not moved during this self-relaxation process, while the conductance was measured as a function of time. The results are summarized in the conductance vs. time plot in Figure 6d. The configurations having the longest lifetimes were found between 10^{-5} and 10^{-6} G_0, with many of these traces reaching the maximum measuring time (120 s). Occasionally, higher conductance values were also found and some of them persist for time scales longer than the average fast-breaking trace. Similar to the fast-breaking measurement method, these observations indicate the presence of a variety of molecular junction configurations, with those displaying the low-conductance values being the most stable ones.

In spite of the fixation of the arrangement of both porphyrins by the additional C−C bond which handicaps the intended mechanical manipulation, the collected breaking traces were analyzed for the appearance of electrode spacing modulated conductance variations. Indeed, in about 2% of the molecular traces recorded by the fast-breaking technique an oscillation of the conductance with increasing electrode distance was observed (Figure S35). However, the seldom appearance of this feature pointing at a response to mechanical manipulation does not yet allow for definite conclusions.

CONCLUSION

The bowl-shaped porphyrin dimer **2** has been synthesized by serendipity, and its 3-fold interlinked bicyclic structure was fully corroborated spectroscopically. Decoration with a pair of peripheral anchor groups provided **1**, making the interlinked

DOI: 10.1021/acs.joc.9b02327
J. Org. Chem. 2020, 85, 118−128

porphyrin architecture suitable for single molecule transport studies. In spite the considerable dimension and the rigidity of the structure, molecular junctions could be obtained in a MCBJ experiment. The transport analyses displayed a large spread of the recorded single molecule traces pointing at a rich variety of configurations and electronic transparencies of the single molecule junctions. Regardless of the fixed arrangement of the interconnected porphyrin scaffold in **1**, the transport data even comprise first indications of mechanosensitive molecular junctions.

We are currently optimizing the molecular design of dimeric porphyrin cyclophanes as model compounds to investigate the interplay between mechanical manipulation and transport behavior in a single molecule junction.

EXPERIMENTAL SECTION

General Remarks. *Reagents and Solvents.* All commercially available compounds were purchased from Sigma-Aldrich, Acros, Apollo Scientific, Alfa Aesar, and Fluorochem and used without further purification. Anhydrous solvents were purchased from Sigma-Aldrich and stored over molecular sieves (4 Å). Column chromatography was performed on silica gel P60 (40−63 μm) from Silicycle, and the solvents were technical grade. TLC was performed with silica gel 60 F254 aluminum sheets with a thickness of 0.25 mm purchased from Merck.

Synthesis. All reactions with reagents that are easily oxidized or hydrolyzed were performed under argon using Schlenk techniques with anhydrous solvents in glassware, which was dried prior to use.

Analytics and Instruments. Recycling gel permeation chromatography (GPC) was performed on a Shimadzu Prominence System equipped with SDV preparative columns from Polymer Standards Service (two Showdex columns in series, 20 × 600 mm each, exclusion limit: 30000 g/mol) with chloroform as solvent. NMR experiments were performed on Bruker Avance III NMR spectrometers operating at 250, 400, 500, or 600 MHz proton frequencies. The instruments were equipped with a direct-observe 5 mm BBFO smart probe (250, 400, and 600 MHz), an indirect-detection 5 mm BBI probe (500 MHz), or a five-channel cryogenic 5 mm QCI probe (600 MHz). All probes were equipped with actively shielded z-gradients (10 A). The chemical shifts are reported in ppm relative to tetramethylsilane or referenced to residual solvent peak and the J values are given in Hz (±0.1 Hz). Standard Bruker pulse sequences were used, and the data was processed on Topspin 3.2 (Bruker) using 2-fold zero-filling in the indirect dimension for all 2D experiments. GC-MS was performed on a Shimadzu GC-MS-2020-SE instrument equipped with a Zebron 5 MS Inferno column, with a temperature range of up to 350 °C. MALDI-TOF mass spectra were recorded on a Bruker MicroFlex LRF spectrometer using *trans*-2-[3-(4-*tert*-butylphenyl)-2-methylpropenylidene]malononitrile (DCTB) as a matrix. High-resolution mass spectra (HRMS) were measured on a Bruker solariX spectrometer with a MALDI source and a Micromass (Waters) AutoSpec Ultima−EI-Sector-MS. Elemental analyses were recorded at room temperature on an Elementar Vario Micro Cube instrument. Melting points were measured on a Büchi M-565 melting point apparatus and are uncorrected. UV/vis absorption spectra were recorded at 20 °C on a JASCO V-770 Spectrophotometer.

NMR Experiments 600 MHz Cryo. All NMR experiments were performed on Bruker Avance III HD four-channel NMR spectrometers operating at 600.13 MHz proton frequency. The instruments were equipped with a cryogenic 5 mm four-channel QCI probe (H/C/N/F) or an RT BBI probe, both with self-shielded z-gradient. The experiments were performed at 298 K, and the temperature was calibrated using a methanol standard showing accuracy within ±0.2 K. The compound was assigned using standard HSQC, HMBC, COSY, and ROESY (mixing time 200 ms) experiments. The diffusion coefficients were determined in an PFGSE (pulsed field gradient spin echo) diffusion experiment using a bipolar gradient pulse sequence. The diffusion time was set to 80 ms, the Eddy current time to 5 ms and the gradient length to 1.5 ms. Gradients with a smoothed square shape (SMSQ10.100) were increased linearly in eight steps from 5 to 95% (2.41 to 45.74 G/cm). The sigmoidal intensity decrease was fitted with a two-parameter fit (I_0 and diffusion coefficient D) with the dosy routine implemented in topspin 3.5 [Bruker Biospin GmbH, 2017]. Five peaks were analyzed for each compound, and the mean and the 95% confidence interval are given in Table S1.

2,2′-((4-(tert-Butyl)phenyl)methylene)bis(1H-pyrrole). According to ref 28, an oven-dried two-necked flask with reflux condenser was charged with freshly distilled pyrrole (250 mL, 3.58 mol, 100 equiv) and 4-*tert*-butylbenzaldehyde (6.00 mL, 35.8 mmol, 1.0 equiv). The mixture was degassed with argon for 20 min. The reaction mixture was heated to 55 °C under the absence of light in an oil bath. $InCl_3$ (792 mg, 3.58 mmol, 0.1 equiv) was added in one portion, and the mixture was stirred at 55 °C for 3 h. NaOH (4.30 g, 107 mmol, 3.0 equiv) was added, and the resulting mixture was stirred at 55 °C overnight. The mixture was filtered over a plug of silica, which was washed with pyrrole. The solvent was removed via distillation. The crude product was purified via recrystallization (ethanol 7:1 water) to obtain the title compound (8.04 g, 28.8 mmol, 81%) as a white powdered solid: TLC (SiO_2, CH_2Cl_2/cyclohexane (1:1), $UV_{254\ nm}$) R_f = 0.13; ^{1}H NMR (400 MHz, CD_2Cl_2, 298 K, δ/ppm) 8.02 (br s, 2H), 7.39−7.31 (m, 2H), 7.19−7.09 (m, 2H), 6.85−6.51 (m, 2H), 6.28−5.99 (m, 2H), 5.99−5.81 (m, 2H), 5.42 (s, 1H); ^{13}C{^{1}H}-NMR (101 MHz, CD_2Cl_2, 298 K, δ/ppm) 150.4 (C_q), 139.9 (C_q), 133.3 (C_q), 128.4 (C_t), 126.1 (C_t), 117.6 (C_t), 108.8 (C_t), 107.3 (C_t), 44.1 (C_{meso}), 34.9 ($C_{s,\ tBu}$), 31.6 ($C_{p,\ tBu}$); GC−MS (EI+, 70 eV) m/z 278 (68) [M^+], 145 (100) [$M^+ - C_{10}H_{14}$].

*4-Bromo-3-((trimethylsilyl)ethynyl)benzaldehyde (**5**).* 4-Bromo-3-iodobenzaldehyde (27.3 g, 87.8 mmol, 1.0 equiv), $Pd(PPh_3)_2Cl_2$ (3.08 g, 4.39 mmol, 0.05 equiv), and CuI (1.02 g, 5.27 mmol, 0.06 equiv) were dissolved in piperidine and THF (200 mL, 1:3 (v:v)), and the mixture was purged with argon for 15 min in a heat gun dried Schlenk tube. A solution of ethynyltrimethylsilane (15.0 mL, 105 mmol, 1.2 equiv) in THF (20 mL) was purged with argon for 5 min and was subsequently transferred into the Schlenk tube via syringe. The reaction mixture was stirred at rt for 3 h. The reaction mixture was filtered over a plug of silica, eluted with CH_2Cl_2. The solvent was removed under reduced pressure, and the residue was subjected to column chromatography (SiO_2, CH_2Cl_2/cyclohexane (2:1) yielding **5** (21.2 g, 75.5 mmol, 86%) as a yellowish oil: TLC (SiO_2, CH_2Cl_2/cyclohexane (2:1), $UV_{254\ nm}$) R_f = 0.30; mp 57 °C; ^{1}H NMR (250 MHz, CD_2Cl_2, 298 K, δ/ppm) 9.93 (s, 1H), 7.96 (d, $^4J_{HH}$ = 2.0 Hz, 1H), 7.78 (d, $^3J_{HH}$ = 8.3 Hz, 1H), 7.66 (dd, $^3J_{HH}$ = 8.3 Hz, $^4J_{HH}$ = 2.0 Hz, 1H), 0.29 (s, 9H); ^{13}C{^{1}H}-NMR (63 MHz, CD_2Cl_2, 298 K, δ/ppm) 190.9 ($C_{C=O}$), 135.9 (C_q), 135.1 (C_t), 133.9 (C_t), 132.7 (C_q), 130.0 (C_t), 126.9 (C_q), 102.2 ($C_{C\equiv C}$), 102.1 ($C_{C\equiv C}$), −0.1 ($C_{p,\ TMS}$); HRMS (ESI, +) m/z calcd for $C_{13}H_{17}BrNaO_2Si$ [M + Na + CH_3OH]$^+$ 335.0073, found 335.0074.

*4-((Triisopropylsilyl)ethynyl)-3-((trimethylsilyl)ethynyl)-benzaldehyde (**4**).* 4-Bromo-3-((trimethylsilyl)ethynyl)benzaldehyde (**5**, 21.2 g, 75.4 mmol, 1.0 equiv), $Pd(PPh_3)_2Cl_2$ (2.65 g, 3.77 mmol, 0.05 equiv), and CuI (879 mg, 4.52 mmol, 0.06 equiv) were dissolved in NEt_3 and toluene (200 mL, 1:3 (v:v)), and the mixture was purged with argon for 15 min in a heat gun dried Schlenk tube. A solution of ethynyltriisopropylsilane (20.3 mL, 90.5 mmol, 1.2 equiv) in toluene (20 mL) was purged with argon for 5 min and was transferred into the Schlenk tube via syringe, subsequently. The reaction mixture was stirred at 80 °C oil bath temperature for 2 h. The reaction mixture was filtered over a plug of silica, eluted with CH_2Cl_2. The solvent was removed under reduced pressure, and the residue was subjected to column chromatography (SiO_2, ethyl acetate/cyclohexane (1:5) yielding **4** (23.3 g, 80.7 mmol, 81%) as a yellowish oil: TLC (SiO_2, ethyl acetate/cyclohexane (1:5), $UV_{254\ nm}$) R_f = 0.53; ^{1}H NMR (400 MHz, CD_2Cl_2, 298 K, δ/ppm) 9.95 (s, 1H), 7.96 (d, $^4J_{HH}$ = 1.6 Hz, 1H), 7.75 (dd, $^3J_{HH}$ = 8.0 Hz, $^4J_{HH}$ = 1.7 Hz, 1H), 7.62 (d, $^3J_{HH}$ = 8.0 Hz, 1H), 1.18−1.14 (m, 21H), 0.26 (s, 9H); ^{13}C{^{1}H}-NMR (101 MHz, CD_2Cl_2, 298 K, δ/ppm) 191.2 (C_{CHO}), 135.9 (C_q), 134.7 (C_t), 134.0 (C_t), 131.6 (C_q), 128.7 (C_t), 126.9 (C_q), 104.9 ($C_{C\equiv C}$), 102.5

DOI: 10.1021/acs.joc.9b02327
J. Org. Chem. 2020, 85, 118−128

($C_{C\equiv C}$), 100.7 ($C_{C\equiv C}$), 100.6 ($C_{C\equiv C}$), 19.1 ($C_{p,\ TIPS}$), 11.8 ($C_{s,\ TIPS}$), 0.1 ($C_{p,\ TMS}$); HRMS (EI, +) *m/z* calcd for $C_{23}H_{34}OSi_2$ $[M]^+$ 382.2148, found 382.2134 (16); calcd for $C_{20}H_{27}OSi_2$ $[M\text{-}i\text{Pr}]^+$ 339.1600, found 339.1591 (66); calcd for $C_{17}H_{21}OSi_2$ $[M - 2i\text{Pr} + H]^+$ 297.1131, found 297.1137 (100).

*5-(2-Bromophenyl)-10,20-bis(4-(tert-butyl)phenyl)-15-(4-((triisopropylsilyl)ethynyl)-3-((trimethylsilyl)ethynyl)phenyl)-porphyrin (**6**).* A solution of 4-((triisopropylsilyl)ethynyl)-3-((trimethylsilyl)ethynyl)benzaldehyde (**4**, 459 mg, 1.20 mmol, 1.0 equiv), 2-bromobenzaldehyde (141 μL, 1.20 mmol, 1.0 equiv), and 2,2′-((4-(*tert*-butyl)phenyl)methylene)bis(1*H*-pyrrole) (668 mg, 2.40 mmol, 2.0 equiv) in CH_2Cl_2 (125 mL) was purged with argon for 20 min in a heat gun dried Schlenk flask at −10 °C which was shielded from light. Trifluoroborane diethyl etherate (0.03 mL, 250 μmol, 0.2 equiv) was added, and the reaction mixture was stirred for 15 min. 2,3-Dichloro-5,6-dicyano-1,4-benzoquinone (599 mg, 2.64 mmol, 2.2 equiv) was added, and the mixture was stirred for 1 h at rt. The reaction mixture was filtered over a plug of silica, and was concentrated under reduced pressure. The residue was subjected to size-exclusion column chromatography (Bio Beads SX3 in toluene) and the collected fractions were analyzed by thin-layer chromatography (SiO_2, ethyl acetate/toluene/cyclohexane (1:1:25)). Crystallization from a concentrated solution of the product comprising fractions in CH_2Cl_2 by top layering with methanol gave **6** (116 mg, 107 μmol, 9%) as a microcrystalline purple solid: TLC (SiO_2, EtOAc/toluene/cyclohexane (1:1:25)) R_f = 0.55; mp > 300 °C; ^{1}H NMR (500 MHz, CD_2Cl_2, 298 K, δ/ppm) 8.91 (d, $^3J_{HH}$ = 4.9 Hz, 4H), 8.83 (d, $^3J_{HH}$ = 4.8 Hz, 2H), 8.70 (d, $^3J_{HH}$ = 4.8 Hz, 2H), 8.34 (dd, $^3J_{HH}$ = 4.7 Hz, 4J_{HH} = 1.8 Hz, 1H), 8.21−8.16 (m, 2H), 8.15−8.09 (m, 4H), 8.05 (dd, $^3J_{HH}$ = 8.0 Hz, 1H), 7.89 (d, $^3J_{HH}$ = 7.8 Hz, 1H), 7.83−7.77 (m, 4H), 7.76−7.68 (m, 2H), 1.61 (s, 18H), 1.29 (s, 21H), 0.24 (s, 9H), −2.80 (s, 2H); ^{13}C{^{1}H}-NMR (126 MHz, CD_2Cl_2, 298 K, δ/ppm) 151.4, 143.2, 142.8, 139.3, 139.0, 135.8, 135.8, 134.9, 134.6, 134.6, 132.5, 131.8, 131.8, 130.6, 128.0, 126.6, 125.6, 124.6, 124.4, 124.4, 121.3, 119.0, 118.7, 105.8, 100.6, 99.3, 96.9, 35.4, 31.9, 19.3, 12.0, 1.3; MALDI-TOF *m/z* = 1081 (100); UV/vis (CH_2Cl_2): λ_{max}[nm] (ε [L·cm^{-1}·mol^{-1}]) = 420 (1.06 × 10^5), 518 (7.44 × 10^3), 549 (3.38 × 10^3), 592 (1.73 × 10^3), 647 (1.42 × 10^3). Anal. Calcd for $C_{68}H_{73}BrN_4Si_2$:C, 75.45; H, 6.80; N, 5.18. Found: C, 75.71; H, 6.80; N, 5.16.

*[5-(2-Bromophenyl)-10,20-bis(4-(tert-butyl)phenyl)-15-(4-((triisopropylsilyl)ethynyl)-3-((trimethylsilyl)ethynyl)phenyl)-porphyrinato]zinc(II) (**7**).* A solution of **6** (149 mg, 138 μmol, 1.0 equiv) and zinc acetate (127 mg, 690 μmol, 5 equiv) in CH_2Cl_2 and methanol (50 mL, 1:1) was stirred at rt for 1 h. The mixture was eluted with CH_2Cl_2 and was washed with satd aq $NaHCO_3$ solution, water, and brine. The aqueous layer was extracted with CH_2Cl_2. The combined organic phases were dried over anhydrous Na_2SO_4 and concentrated under reduced pressure yielding **7** (153 mg, 134 μmol, 97%) as microcrystalline pinkish solid: TLC (SiO_2, EtOAc/toluene/cyclohexane (1:1:25)) R_f = 0.36; mp > 300 °C; ^{1}H NMR (600 MHz, CD_2Cl_2, 298 K, δ/ppm) 9.00 (d, $^3J_{HH}$ = 4.7 Hz, 4H), 8.91 (d, $^3J_{HH}$ = 4.7 Hz, 2H), 8.78 (d, $^3J_{HH}$ = 4.7 Hz, 2H), 8.34 (dd, $^3J_{HH}$ = 7.0 Hz, $^4J_{HH}$ = 1.8 Hz, 1H), 8.21−8.08 (m, 6H), 8.07−8.02 (m, 1H), 7.88 (dd, $^3J_{HH}$ = 7.9 Hz, $^4J_{HH}$ = 1.7 Hz, 1H), 7.83−7.76 (m, 4H), 7.74−7.68 (m, 2H), 1.62 (s, 18H), 1.28 (s, 21H), 0.23 (d, *J* = 0.7 Hz, 9H); ^{13}C{^{1}H}-NMR (126 MHz, CD_2Cl_2, 298 K, δ/ppm) 151.3, 151.1, 150.3, 150.2, 143.8, 143.5, 140.0, 139.0, 135.7, 134.8, 134.5, 133.2, 132.9, 132.4, 132.0, 131.7, 131.6, 130.4, 128.0, 126.5, 125.4, 124.9, 124.2, 122.2, 119.9, 111.0, 105.9, 104.0, 96.7, 0 35.4, 32.0, 19.3, 12.0, 1.3; MALDI-TOF *m/z* = 1144 (100); UV/vis (CH_2Cl_2) λ_{max}[nm] (ε [L·cm^{-1}·mol^{-1}]) = 422 (1.55 × 10^6), 505 (2.93 × 10^4), 549 (8.21 × 10^4), 588 (2.82 × 10^4). Anal. Calcd for $C_{68}H_{71}BrN_4Si_2Zn$:C, 71.28; H, 6.25; N, 4.89; found: C, 71.43; H, 6.44; N, 4.82;

*[5-(2-Bromophenyl)-10,20-bis(4-(tert-butyl)phenyl)-15-(3-ethynyl-4-((triisopropylsilyl)ethynyl)phenyl)porphyrinato]zinc(II) (**3**).* A solution of **7** (150 mg, 131 μmol, 1.0 equiv) and K_2CO_3 (181 mg, 1.31 mmol, 10 equiv) in CH_2Cl_2 and methanol (50 mL, 1:1) was stirred at rt for 1 h. The mixture was eluted with CH_2Cl_2 and was washed with satd aq $NaHCO_3$ solution, water, and brine. The aqueous layer was extracted with CH_2Cl_2. The combined organic phases were dried over anhydrous Na_2SO_4 and concentrated under reduced pressure yielding **3** (139 mg, 129 mmol, 99%) as a pinkish microcrystalline solid: TLC (SiO_2, EtOAc/toluene/cyclohexane (1:1:25)) R_f = 0.30; mp > 240 °C dec; ^{1}H NMR (250 MHz, CD_2Cl_2, 298 K, δ/ppm) 9.00 (d, $^3J_{HH}$ = 4.7 Hz, 4H), 8.92 (d, $^3J_{HH}$ = 4.8 Hz, 2H), 8.79 (d, $^3J_{HH}$ = 4.7 Hz, 2H), 8.36 (dd, $^3J_{HH}$ = 6.6 Hz, $^4J_{HH}$ = 1.7 Hz, 1H), 8.22−8.15 (m, 4H), 8.14−8.07 (m, 2H), 8.05 (dd, $^3J_{HH}$ = 7.3 Hz, $^4J_{HH}$ 2.0 Hz, 1H), 7.90 (dd, $^3J_{HH}$ = 7.8 Hz, $^4J_{HH}$ 1.5 Hz, 1H), 7.83−7.76 (m, 4H), 7.76−7.68 (m, 2H), 3.41 (d, *J* = 0.9 Hz, 1H), 1.62 (s, 18H), 1.27 (s, 21H); *No* ^{13}C{^{1}H}-NMR *spectrum was recorded due to the low solubility of* **3**; MALDI-TOF *m/z* = 1071 (100); UV/vis (CH_2Cl_2): λ_{max}[nm] (ε [L·cm^{-1}·mol^{-1}]) = 422 (5.17 × 10^5), 507 (2.52 × 10^2), 550 (1.82 × 10^4), 589 (1.80 × 10^3). Anal. Calcd for $C_{65}H_{63}BrN_4SiZn$:C, 72.72; H, 5.91; N, 5.22. Found: C, 73.06; H, 6.26; N, 4.97;

*[0$_3$](13,10-(3-(2-)),20-(2-))-5,15-Bis(4-(tert-butyl)phenyl)-10-(3-ethynyl-4-((triisopropylsilyl)ethynyl)phenyl)-20-phenylporphyrinato]zinc(II) (**2**).* A dry and degassed solution of **3** (60.1 mg, 56.0 μmol, 1.0 equiv) in toluene (50 mL) was added to a dry and degassed solution of $Pd(PPh_3)_4$ (64.7 mg, 56.0 μmol, 1.0 equiv), dppf (32.0 mg, 56.0 μmol, 1.0 equiv), and CuI (11.7 mg, 61.6 μmol, 1.1 equiv) in NEt_3 (30 mL) and toluene (50 mL), and the mixture was placed in a preheated oil bath and was stirred vigorously at 110 °C for 2 d. The mixture was filtered over silica eluted with toluene. The solvent was removed under reduced pressure and the residue subjected to size-exclusion column chromatography (Bio Beads SX3 in toluene), followed by size-exclusion column chromatography (Bio Beads SX1 in toluene) followed by automated GPC in chloroform. Finally, the compound was subjected to column chromatography using freshly distilled solvents (SiO_2, ethyl acetate/toluene/cyclohexane (1:1:15) yielding **2** (3.21 mg, 1.62 μmol, 5.7%) as a green solid: TLC (SiO_2, EtOAc/toluene/cyclohexane (1:1:10)) R_f = 0.50.; ^{1}H NMR (600 MHz, benzene-d_6, 298 K, δ/ppm) 9.08 (d, $^3J_{HH}$ = 4.8 Hz, 1H, H-11), 8.88 (d, $^3J_{HH}$ = 4.5 Hz, 1H, H-12), 8.74 (d, $^3J_{HH}$ = 4.4 Hz, 1H, H-44), 8.69 (d, $^3J_{HH}$ = 4.6 Hz, 1H, H-22), 8.51 (d, $^3J_{HH}$ = 4.6 Hz, 1H, H-23), 8.46 (d, $^3J_{HH}$ = 4.2 Hz, 1H, H-45), 8.46 (s, 1H, H-31), 8.16 (m, 2H, H-16/H-38), 8.14 (m, 2H. H-20/H-42), 8.13 (s, 1H, H-33), 7.99 (d, $^3J_{HH}$ = 7.4 Hz, 1H, H-7), 7.76 (dd, $^3J_{HH}$ = 7.7 Hz, $^4J_{HH}$ = 1.9 Hz, 1H, H-27), 7.69 (m, 1H, H-17), 7.68 (m, 1H, H-39), 7.65 (m, 1H, H-19), 7.64 (m, 1H, H-41), 7.56 (d, $^3J_{HH}$ = 7.7 Hz, 1H, H-28), 7.16 (d, $^3J_{HH}$ = 7.0 Hz, 1H, H-4), 6.87 (t, $^3J_{HH}$ = 7.1 Hz, 1H, H-6), 6.78 (t, $^3J_{HH}$ = 7.4 Hz, 1H, H-5), 1.51 (s, 9H, H-48), 1.49 (s, 9H, H-54), 1.30 (d, $^3J_{HH}$ = 6.9 Hz, 16H, H-51), 1.23 (h, $^3J_{HH}$ = 7.4 Hz, 3H, H-52).; ^{13}C{^{1}H}-NMR (151 MHz, over 2D-NMR [HMBC, HSQC], benzene-d_6, 298 K, δ/ppm)161.5 (C-35), 155.2 (C-32), 152.5 (C-21), 152.2 (C-8), 151.9 (C-43), 151.4 (C-13), 150.6 (C-40), 150.6 (C-18), 150.3 (C-46), 149.4 (C-24), 148.5 (C-10), 147.3 (C-34), 143.2 (C-26), 142.7 (C-33), 140.3 (C-15), 139.0 (C-37), 138.4 (C-31), 135.6 (C-12), 134.8 (C-38), 134.7 (C-42), 134.64 (C-27), 134.60 (C-16), 134.5 (20), 132.3 (C-23), 132.02 (C-22), 131.95 (C-44), 131.4 (C-28), 130.8 (C-45), 129.9 (C-6), 128.4 (C-5), 126.9 (C-29), 126.8 (C-11), 126.1 (C-14/C-36), 125.2 (C-7), 124.7 (C-4), 124.29 (C-41), 124.28 (C-39), 124.26 (C-30), 124.19 (C-19), 124.18 (C-17), 121.4 (C-14/C-36), 121.3 (C-25), 114.0 (C-9), 105.8 (C-49), 97.7 (C-2/C-50), 95.6 (C-2/C-50), 82.4 (C-1), 35.0 (C-47/C-53), 31.81 (C-54), 31.82 (C-48), 19.1 (C-51), 11.8 (C-52); HR-MALDI-TOF *m/z* $[M^+]$ Calcd for $C_{130}H_{122}N_8Si_2Zn_2$ 1978.7908; Found 1978.7912; UV/vis (CH_2Cl_2) λ_{max}[nm]) = 420, 447, 470, 508, 550, 593, 689.

DOI: 10.1021/acs.joc.9b02327
J. Org. Chem. 2020, 85, 118−128

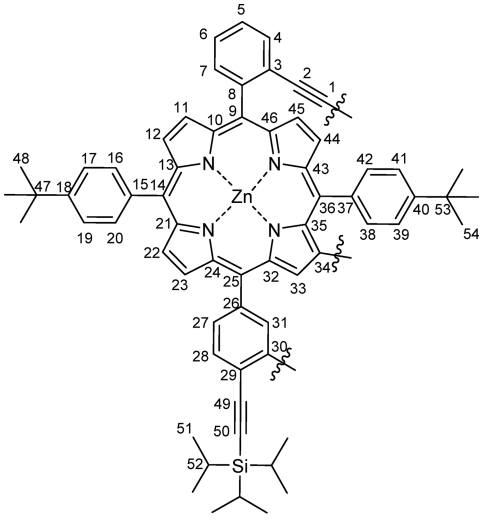

2

*[0$_3$](13,10-(3-(2-)),20-(2-))-[5,15-Bis(4-(tert-butyl)phenyl)-10-(3-ethynyl-4-(p-ethanthioatephenylethynyl)phenyl)-20-phenylporphyrinato]zinc(II) (**1**).* To a degassed solution of **2** (1.2 mg, 0.6 μmol, 1.0 equiv) in THF (5 mL) was added a solution of TBAF in THF (1 M, 0.03 mL, 50 equiv) at rt, and the mixture was stirred for 1 h. The mixture was filtered over silica eluted with CH_2Cl_2. The solvent was removed under reduced pressure, and the residue was redissolved in dry THF (3 mL). The mixture was degassed and was transferred into a previously degassed solution of $Pd(PPh_3)_4$ (34.9 μg, 0.03 μmol, 0.05 equiv), CuI (6.90 μg, 0.036 μmol, 0.06 equiv), and *S*-(4-Iodophenyl)ethanethioate (0.50 mg, 1.81 μmol, 3 equiv) in NEt_3 (1 mL), via syringe. The mixture was stirred for 1 h at rt. Toluene was added, and the mixture was filtered over a plug of silica eluted with CH_2Cl_2. The filtrate was concentrated and subjected to size-exclusion column chromatography (Bio Beads SX3 in toluene) to give **1** (1.0 mg, 0.52 μmol, 84%) as a green solid: TLC (SiO_2, ethyl acetate/toluene/cyclohexane (1:1:5)) R_f = 0.55; HR-MALDI-TOF *m*/*z* [M^+] calcd for $C_{128}H_{94}N_8O_2S_2Zn_2$ 1966.5519, found 1966.5654; UV/vis ($CHCl_3$) λ_{max}[nm]) = 428, 441, 473, 513, 554, 597, 694.

■ ASSOCIATED CONTENT

Supporting Information

The Supporting Information is available free of charge on the ACS Publications website at DOI: 10.1021/acs.joc.9b02327.

Synthetic overview, NMR spectra, HR-MS reports, UV–vis spectra, elemental analysis reports, example single trace of conductance experiments, and calculation details (PDF)

■ AUTHOR INFORMATION

Corresponding Author

*E-mail: marcel.mayor@unibas.ch. Phone: +41 207 10 06.

ORCID

Davide Stefani: 0000-0002-9406-9265
Daniel Häussinger: 0000-0002-4798-0072
Herre S. J. van der Zant: 0000-0002-5385-0282
Diana Dulić: 0000-0002-8302-5507
Marcel Mayor: 0000-0002-8094-7813

Notes

The authors declare no competing financial interest.

■ ACKNOWLEDGMENTS

This study was supported by the EU through a RISE(DAFNEOX) project, SEP 210165479, and partially funded by the FET open project QuIET (no. 767187). The device fabrication was done at the Kavli Nanolab at Delft. Generous financial support by the Swiss National Science Foundation (SNF Grant No. 200020-178808) is gratefully acknowledged. M.M. acknowledges support by the 111 project (90002-18011002). D.D. acknowledges support by Fondecyt Regular Project (Grant No. 1181080). We thank Chuwei Hsu and Alfredo Rates Soriano for their help with the measurements and the clustering, respectively.

■ REFERENCES

(1) Aviram, A.; Ratner, M. A. Molecular Rectifiers. *Chem. Phys. Lett.* **1974**, *29* (2), 277–283.
(2) Xiang, D.; Wang, X.; Jia, C.; Lee, T.; Guo, X. Molecular-Scale Electronics: From Concept to Function. *Chem. Rev.* **2016**, *116* (7), 4318–4440.
(3) Sun, L.; Diaz-Fernandez, Y. A.; Gschneidtner, T. A.; Westerlund, F.; Lara-Avila, S.; Moth-Poulsen, K. Single-Molecule Electronics: From Chemical Design to Functional Devices. *Chem. Soc. Rev.* **2014**, *43* (21), 7378–7411.
(4) Untiedt, C.; Rubio Bollinger, G.; Vieira, S.; Agraït, N. Quantum Interference in Atomic-Sized Point Contacts. *Phys. Rev. B: Condens. Matter Mater. Phys.* **2000**, *62* (15), 9962–9965.
(5) Konda, S. S. M.; Avdoshenko, S. M.; Makarov, D. E. Exploring the Topography of the Stress-Modified Energy Landscapes of Mechanosensitive Molecules. *J. Chem. Phys.* **2014**, *140* (10), 104114.
(6) Xia, J. L.; Diez-Perez, I.; Tao, N. J. Electron Transport in Single Molecules Measured by a Distance-Modulation Assisted Break Junction Method. *Nano Lett.* **2008**, *8* (7), 1960–1964.
(7) Vonlanthen, D.; Mishchenko, A.; Elbing, M.; Neuburger, M.; Wandlowski, T.; Mayor, M. Chemically Controlled Conductivity: Torsion-Angle Dependence in a Single-Molecule Biphenyldithiol Junction. *Angew. Chem., Int. Ed.* **2009**, *48* (47), 8886–8890.
(8) Elbing, M.; Ochs, R.; Koentopp, M.; Fischer, M.; von Hänisch, C.; Weigend, F.; Evers, F.; Weber, H. B.; Mayor, M. A Single-Molecule Diode. *Proc. Natl. Acad. Sci. U. S. A.* **2005**, *102* (25), 8815–8820.
(9) Gerhard, L.; Edelmann, K.; Homberg, J.; Valášek, M.; Bahoosh, S. G.; Lukas, M.; Pauly, F.; Mayor, M.; Wulfhekel, W. An Electrically Actuated Molecular Toggle Switch. *Nat. Commun.* **2017**, *8*, 14672.
(10) Franco, I.; George, C. B.; Solomon, G. C.; Schatz, G. C.; Ratner, M. A. Mechanically Activated Molecular Switch through Single-Molecule Pulling. *J. Am. Chem. Soc.* **2011**, *133* (7), 2242–2249.
(11) Ferri, N.; Algethami, N.; Vezzoli, A.; Sangtarash, S.; McLaughlin, M.; Sadeghi, H.; Lambert, C. J.; Nichols, R. J.; Higgins, S. J. Hemilabile Ligands as Mechanosensitive Electrode Contacts for Molecular Electronics. *Angew. Chem., Int. Ed.* **2019**, *131*, 2–9.
(12) Stefani, D.; Perrin, M.; Gutiérrez-Cerón, C.; Aragonès, A. C.; Labra-Muñoz, J.; Carrasco, R. D. C.; Matsushita, Y.; Futera, Z.; Labuta, J.; Ngo, T. H.; et al. Mechanical Tuning of Through-Molecule Conductance in a Conjugated Calix[4]Pyrrole. *ChemistrySelect* **2018**, *3* (23), 6473–6478.
(13) Li, Y.; Haworth, N. L.; Xiang, L.; Ciampi, S.; Coote, M. L.; Tao, N. Mechanical Stretching-Induced Electron-Transfer Reactions and Conductance Switching in Single Molecules. *J. Am. Chem. Soc.* **2017**, *139* (41), 14699–14706.
(14) Frisenda, R.; Harzmann, G. D.; Celis Gil, J. A.; Thijssen, J. M.; Mayor, M.; van der Zant, H. S. J. Stretching-Induced Conductance Increase in a Spin-Crossover Molecule. *Nano Lett.* **2016**, *16* (8), 4733–4737.
(15) Frisenda, R.; Janssen, V. A. E. C.; Grozema, F. C.; van der Zant, H. S. J.; Renaud, N. Mechanically Controlled Quantum Interference in Individual π-Stacked Dimers. *Nat. Chem.* **2016**, *8* (12), 1099–1104.
(16) Stefani, D.; Weiland, K. J.; Skripnik, M.; Hsu, C.; Perrin, M. L.; Mayor, M.; Pauly, F.; van der Zant, H. S. J. Large Conductance Variations in a Mechanosensitive Single-Molecule Junction. *Nano Lett.* **2018**, *18* (9), 5981–5988.

DOI: 10.1021/acs.joc.9b02327
J. Org. Chem. 2020, 85, 118–128

(17) Yang, H.; Liu, J.; Wen, X.; Lu, C. Molecular Mechanism of Photosystem I Assembly in Oxygenic Organisms. *Biochim. Biophys. Acta, Bioenerg.* **2015**, *1847* (9), 838−848.
(18) Balaban, T. S. Tailoring Porphyrins and Chlorins for Self-Assembly in Biomimetic Artificial Antenna Systems. *Acc. Chem. Res.* **2005**, *38* (8), 612−623.
(19) Horn, S.; Dahms, K.; Senge, M. O. Synthetic Transformations of Porphyrins − Advances 2004−2007. *J. Porphyrins Phthalocyanines* **2008**, *12* (10), 1053−1077.
(20) Jurow, M.; Schuckman, A. E.; Batteas, J. D.; Drain, C. M. Porphyrins as Molecular Electronic Components of Functional Devices. *Coord. Chem. Rev.* **2010**, *254* (19−20), 2297−2310.
(21) Sedghi, G.; Sawada, K.; Esdaile, L. J.; Hoffmann, M.; Anderson, H. L.; Bethell, D.; Haiss, W.; Higgins, S. J.; Nichols, R. J. Single Molecule Conductance of Porphyrin Wires with Ultralow Attenuation. *J. Am. Chem. Soc.* **2008**, *130* (27), 8582−8583.
(22) Li, Z.; Park, T.-H.; Rawson, J.; Therien, M. J.; Borguet, E. Quasi-Ohmic Single Molecule Charge Transport through Highly Conjugated Meso-to-Meso Ethyne-Bridged Porphyrin Wires. *Nano Lett.* **2012**, *12* (6), 2722−2727.
(23) Leary, E.; Limburg, B.; Alanazy, A.; Sangtarash, S.; Grace, I.; Swada, K.; Esdaile, L. J.; Noori, M.; González, M. T.; Rubio-Bollinger, G.; et al. Bias-Driven Conductance Increase with Length in Porphyrin Tapes. *J. Am. Chem. Soc.* **2018**, *140* (40), 12877−12883.
(24) Li, Z.; Smeu, M.; Ratner, M. A.; Borguet, E. Effect of Anchoring Groups on Single Molecule Charge Transport through Porphyrins. *J. Phys. Chem. C* **2013**, *117* (29), 14890−14898.
(25) El Abbassi, M.; Zwick, P.; Rates, A.; Stefani, D.; Prescimone, A.; Mayor, M.; van der Zant, H. S. J.; Dulić, D. Unravelling the Conductance Path through Single-Porphyrin Junctions. *Chem. Sci.* **2019**, *10*, 8299−8305.
(26) Frisch, M. J.; Trucks, G. W.; Schlegel, H. B.; Scuseria, G. E.; Robb, Ma.; Cheeseman, J. R.; Scalmani, G.; Barone, V.; Mennucci, B.; Petersson, G. A. et al. *Gaussian 09*, Revision D. 01, Gaussian, Inc.: Wallingford, CT, 2009.
(27) Dogutan, D. K.; Zaidi, S. H. H.; Thamyongkit, P.; Lindsey, J. S. New Route to ABCD-Porphyrins via Bilanes. *J. Org. Chem.* **2007**, *72* (20), 7701−7714.
(28) Hunter, C. A.; Sanders, J. K. M.; Stone, A. J. Exciton Coupling in Porphyrin Dimers. *Chem. Phys.* **1989**, *133* (3), 395−404.
(29) Kasha, M.; Rawls, H. R.; Ashraf El-Bayoumi, M. The Exciton Model in Molecular Spectroscopy. *Pure Appl. Chem.* **1965**, *11* (3), 371−392.
(30) Hiroto, S.; Miyake, Y.; Shinokubo, H. Synthesis and Functionalization of Porphyrins through Organometallic Methodologies. *Chem. Rev.* **2017**, *117* (4), 2910−3043.
(31) Ikeda, T.; Aratani, N.; Easwaramoorthi, S.; Kim, D.; Osuka, A. Meso-β Doubly Linked Zn(II) Porphyrin Trimers: Distinct Anti-versus-Syn Effects on Their Photophysical Properties. *Org. Lett.* **2009**, *11* (14), 3080−3083.
(32) Nakamura, Y.; Jang, S. Y.; Tanaka, T.; Aratani, N.; Lim, J. M.; Kim, K. S.; Kim, D.; Osuka, A. Two-Dimensionally Extended Porphyrin Tapes: Synthesis and Shape-Dependent Two-Photon Absorption Properties. *Chem. - Eur. J.* **2008**, *14* (27), 8279−8289.
(33) Nakamura, Y.; Aratani, N.; Shinokubo, H.; Takagi, A.; Kawai, T.; Matsumoto, T.; Yoon, Z. S.; Kim, D. Y.; Ahn, T. K.; Kim, D.; et al. A Directly Fused Tetrameric Porphyrin Sheet and Its Anomalous Electronic Properties That Arise from the Planar Cyclooctatetraene Core. *J. Am. Chem. Soc.* **2006**, *128* (12), 4119−4127.
(34) Richert, S.; Limburg, B.; Anderson, H. L.; Timmel, C. R. On the Influence of the Bridge on Triplet State Delocalization in Linear Porphyrin Oligomers. *J. Am. Chem. Soc.* **2017**, *139* (34), 12003−12008.
(35) Martin, C. A.; Ding, D.; van der Zant, H. S. J.; van Ruitenbeek, J. M. Lithographic Mechanical Break Junctions for Single-Molecule Measurements in Vacuum: Possibilities and Limitations. *New J. Phys.* **2008**, *10* (6), 065008.
(36) Martin, C. A.; Smit, R. H. M.; van Egmond, R.; van der Zant, H. S. J.; van Ruitenbeek, J. M. A Versatile Low-Temperature Setup for the Electrical Characterization of Single-Molecule Junctions. *Rev. Sci. Instrum.* **2011**, *82* (5), 053907.
(37) Frisenda, R.; Stefani, D.; van der Zant, H. S. J. Quantum Transport through a Single Conjugated Rigid Molecule, a Mechanical Break Junction Study. *Acc. Chem. Res.* **2018**, *51* (6), 1359−1367.
(38) Frisenda, R.; Perrin, M. L.; Valkenier, H.; Hummelen, J. C.; van der Zant, H. S. J. Statistical Analysis of Single-Molecule Breaking Traces. *Phys. Status Solidi B* **2013**, *250* (11), 2431−2436.
(39) Tsutsui, M.; Shoji, K.; Taniguchi, M.; Kawai, T. Formation and Self-Breaking Mechanism of Stable Atom-Sized Junctions. *Nano Lett.* **2008**, *8* (1), 345−349.
(40) Cabosart, D.; El Abbassi, M.; Stefani, D.; Frisenda, R.; Calame, M.; van der Zant, H. S. J.; Perrin, M. L. A Reference-Free Clustering Method for the Analysis of Molecular Break-Junction Measurements. *Appl. Phys. Lett.* **2019**, *114* (14), 143102.

DOI: 10.1021/acs.joc.9b02327
J. Org. Chem. 2020, 85, 118−128